Advanced **S**olar **T**racking and **R**over **O**bservation **C**ommunication

A.S.T.R.O.COM.

Alex Fiset, Pedro Kasprzykowski, Stephen Martin, Binh Pham

Dept. of Electrical Engineering and Computer Science, University of Central Florida, Orlando, Florida, 32816-2450

Florida Space Institute Orlando, Florida, 32826

***Abstract* — The ASTROCOM project, developed in collaboration the Florida Space Institute (FSI), addresses the challenge of exploring permanently shaded regions on the lunar surface. Comprising heliostat and communication beacon towers, ASTROCOM enables wireless transmission of power and information to and from rovers within these shaded areas. The Heliostat tower utilize a reflector to redirect sunlight into the craters, powering solar assets and illuminating shaded regions, while also enabling a communication network. A portable communication beacon, intended to be deployed by rovers, a facilitate communication between the heliostat towers and rovers, overcoming obstacles within the craters. This document outlines the design process, technologies, implementation, and testing results of ASTROCOM.**

***Index Terms* — Fresnel reflection, motor coordination, wireless mesh networks, solar panels, solar energy, batteries**

I. Introduction

ASTROCOM marks a significant advancement in space exploration technology, presenting a sophisticated solar reflector system integrated with a mesh network communication protocol. This project aims to enhance energy harnessing and communication capabilities in extraterrestrial environments. By delving into the detailed design and implementation of ASTROCOM, this paper sheds light on its components, testing procedures, and potential for further improvement.

At the core of ASTROCOM lies a blend of advanced technologies meticulously crafted to tackle the challenges of space exploration. By combining state-of-the-art hardware components with sophisticated software algorithms and Zigbee communication protocols, ASTROCOM offers efficient solar tracking and seamless communication across vast distances in space. As subsequent sections unravel the system's architecture and operational intricacies, ASTROCOM highlights the role of innovation in pushing the boundaries of space exploration, promising new capabilities for future missions beyond Earth.

II. Overview

This paper serves to provide a description of ASTROCOM project. The system components are first summarized in III, then the hardware and software implementation are discussed in IV and V. Following is the discussion of the changes made during testing in VI, and final conclusions presented in VII.

III. System Components

The overall system can be broken down into parts for further explanation of the entire project. The following parts that were designed or purchased compose the entire system.

A. MCU

The ESP32-C6 microcontroller serves as the main control center of the system with its dual core processor and ample flash memory. The chip also has on board Zigbee communication. These aspects allow the microcontroller to balance handling all the various library dependencies within the code and running several motors in accordance with light sensor readings and being attached to the Zigbee network so that commands may be received and sent.

B. Voltage Regulators

The TPS54JA20 IC regulator used is a small high-efficiency synchronous buck converter. Two of these regulators were used to step down the 12V supply from the charge controller down to 5V and 3.3V for the MCU, servos and other peripherals. This small IC has proven to be a powerful regulator and runs cool even under high loads. The regulator offers high efficiency, which is ideal in the context of space exploration and renewable energy. This IC can provide a maximum of 12A, which is more than sufficient for the systems supplied.

C. Solar Panel

The Renogy RNG-50D-SS, a 50W rated panel, was used to ensure a power surplus during standard operation. The combination of low price, weight, and high-power output, reliability and performance in low-light conditions made it effective. Additionally, the availability of detailed datasheets and IV curve data for the Renogy panel benefited the project during testing. The panel is rated for 50W, providing a V_{oc} of 22.2V and an I_{sc} of 2.9A. At the optimum power point the panel operates at a V_{mp} of 18.6V and an I_{mp} of 2.6A.

D. Charge Controller

SMARAAD's SR11004 charge controller was used for the project. The charge controller offers charge control modes for different battery chemistries. The charge controller also supports up to 30A at 12V through the device. This device serves to charge the LiFePo battery and step down the voltage from the solar panel to provide a steady 12V for the stepper and the 5V and 3.3V regulators.

E. Battery

The batteries used for ASTROCOM are 2 12V 7Ah $LiFePo_4$ batteries from Howell Energy. One is utilized to provided power for the communication beacon, and the other serves to provided power for the heliostat during low-light conditions. The battery has its own internal BMS, which prevents over and under voltage conditions. This is beneficial during testing to increase safety and reduce risk of improper charging. The 7Ah supplied is more than enough for both systems, as the communication beacon has very little power draw by design, and the heliostat will draw power from the solar panel for the vast majority of operation.

F. Light Sensors

The VEML7700 light sensors were used on our sensor board due to its superior performance across various criteria, such as high lux value, low power consumption, and compact size, all of which are essential for our project requirements. Its high maximum lux value of over 100,000 is particularly crucial as it allows for precise positioning of the mirror to optimize solar energy absorption. The current draw is a minimal 0.45mA which allows for battery power to be saved during operations. Lastly, the overall size of the sensor can be measured by the area which is a minute $15.98mm^2$

G. Motors and Motor Drivers

Three DS3225 servo motors control the x and y axis of the mirror for light reflection; and the vertical rotation of sensors to tracing sun light. Servos have high torque compared to its small size and have accurate precision for light weight components. The w axis rotation of the whole tower is heavier, which requires a NEMA 23 stepper motor, and the precision of rotation are not a requirement.

A PCA9685 chip controls all servo motors through I2C communication bus. The chip switching the required PWM to rotate each servo into a calculated position by the ESP32-C6 MCU. Through calculations a SPI signals output to TB6560 chip to control the stepper motor. To operate with high torque, the stepper required above 2A, which TB6560 provide along with 24V rating.

H. Mechanical Parts

A plate of polymethyl methacrylate was cut in to a 2 ft diameter circle to perform as a mirror backing due to the high stability and flexibility. Then a layer of mylar applied on top using adhesive to give a reflective surface to reflect sun light. The reflector attaches to a housing and arm to be control by servo motor in vertical and horizonal axis.

Five sensors were used to calculate the direction of sun light; hence a partition is needed to distinguish the amount of light at each sensor. The sensor board divided into five sections, the peripheral quadrant used to find the left, right, up and down ray tracing. The middle section used to confirm the direct sunlight ray input.

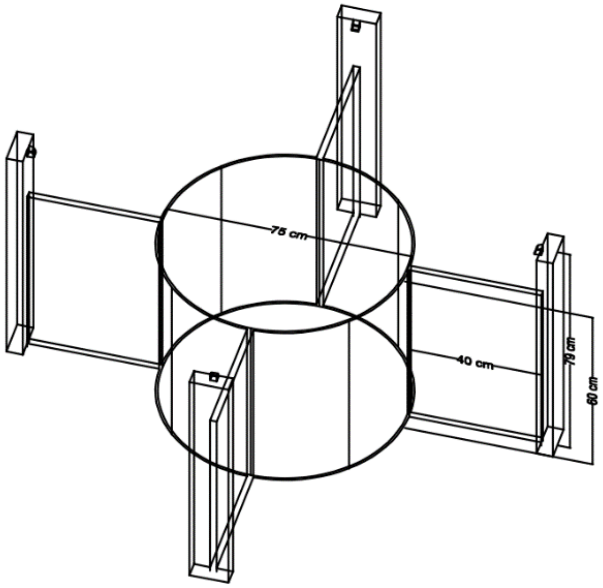

Fig. 1. Sensor's partition design and measurement.

Multiple board's housings used to contain MCU, stepper and servo controller PCB boards. The housing of stepper contained air vent for heat dissipation from heat sink due to the high amperage pull from the stepper motor. Further development of fan implementation can be attached directly on to the housing box.

The reflector tower's base is made from 3 sheets of 3/8ths inch plywood. It features a "lazy-susan" turntable bearing to enable the tower to rotate freely. To prevent balance issues, roller bearings were placed between the base of the turntable and the top of the base. The base also stores the stepper motor, geared 2-1, to reduce the torque required from the stepper. A 4-conductor slipring is utilized to transfer signals down to the stepper without the cabling twisting. 3D printed components such as the gears, stand, and housings, helped reduce the total cost of the project and enabled iterative design.

The communication beacon is an enclosure is an IP65 rated enclosure, which stores a Howell Energy LiFePo

battery, 12-5V regulator and ESP-C6 Devkit board. The plastic enclosure ensures that the Zigbee communication is unimpeded and keeps the internal components free from dust or humidity during testing.

I. Wireless Communication Protocol

Zigbee was used to implement the mesh network in the project. While supporting theoretically infinite scalability with the addition of more router devices, Zigbee is also low power and provides outstanding range on a location like the moon. The communication rate is not a worry, reliability is preferred. Zigbee provides the backbone for a stable, reliable and scalable mesh network between rovers, towers and any additional nodes on the moon's surface.

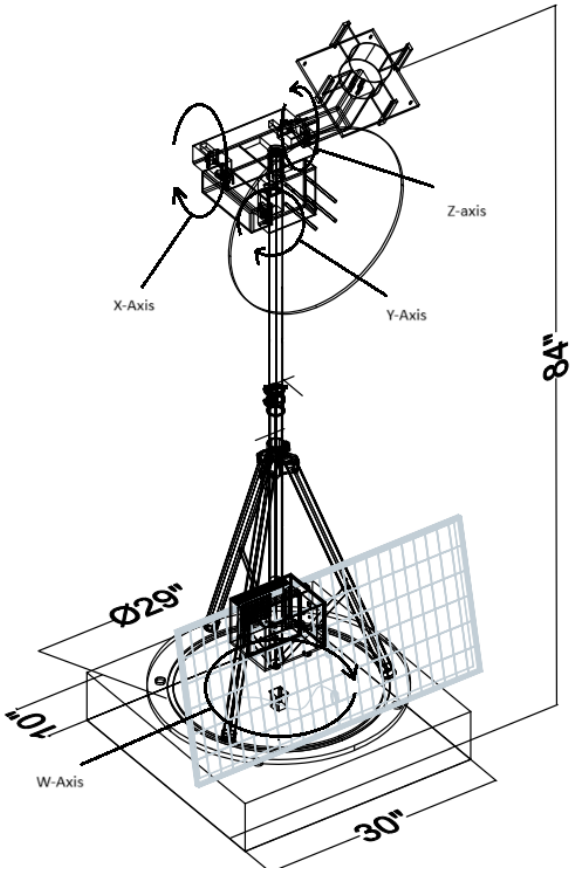

Fig. 2. Reflector Tower design and measurements; Including a base with lazy Sussan design, boards housing at the bottom, solar panel, tripod, top board housing. Four rotation axis w, x, y and z are labeled.

IV. HARDWARE

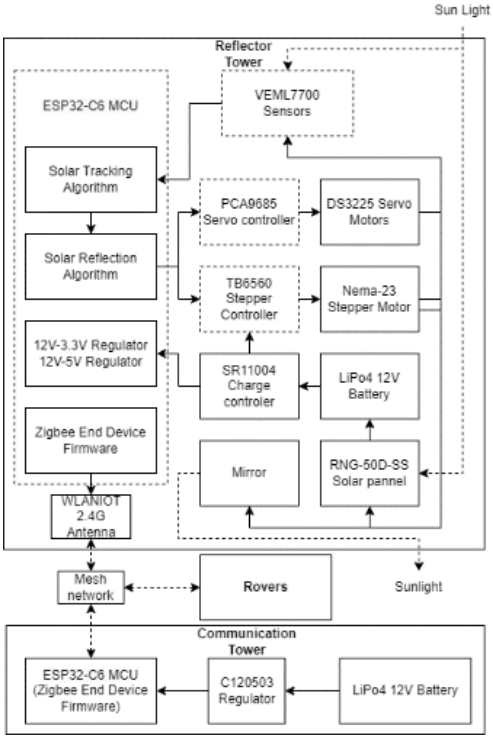

Fig. 3. Overall hardware diagram

A. Reflection control

The heliostat reflection angle can be calculated using an algorithm; according to Figure 4 and information from Alberto [1], we can realize (1) such that:

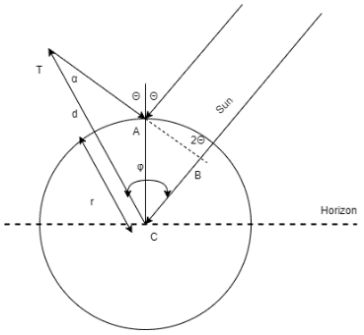

Fig. 4. Reflection of light diagram, the Horizon would represent a mirror surface.

$$\frac{d}{r} = \left| \frac{\sin\left(\left(\frac{x}{2^n}+2\right)\right)\phi}{\sin\left(\left(\frac{x-2^n+1}{2^n+1}\right)\phi\right)} \right|. \quad (1)$$

This is based on the law of sine to calculate the angle, TCB at the center of the reflection circle, ϕ is the rotation

origin, and T is the target location. The angle variable θ is unknown and can be calculated using geometry such that $\frac{\phi}{2}$ is the limit of an iterative process.

An algorithm can be realized as (3), with n being the rotating process iteration. This algorithm is the base to find the highest angle of the lumen to the reflector. However, the mirror needs to be rotated in 2 different axes based on incoming requests rather than automatically shine to a fixed position—an additional algorithm based on the grid network to pinpoint a location.

An additional algorithm of rotation needs to be used to control the reflector. The horizontal axis W of the whole tower will rotate according to the sun's position. An additional motor must turn the mirror to control the X and Y axis to point to a pre-determined location based on the network algorithm.

$$\frac{d}{r} = \frac{\sin(\theta)}{\sin(2\theta - \phi)}. \quad (2)$$

B. The PCB Design

For ASTROCOM, four unique PCBs were designed: an MCU board, servo controller board, sensor board, and stepper board.

1) MCU: The most complex was the MCU board. The MCU board was designed to interact with four different devices: the sensor board, the servo controller board, the stepper controller and a laptop for programing. This required five connectors, four for the peripheral devices and one for the 12V line from the charge controller. For the laptop connector, a USBC connector and a USB/UART converter were utilized. Also included on this connector was a 5V to 3.3V regulator with a jumper bridge, enabling the 3.3V line to be powered directly from the laptop without external power supply during testing. This proved useful and special attention was paid to avoid connecting the 5V lines from the USBC and the board's 5V line, as well as avoiding connecting both 12V to 3.3V regulator and the 5V to 3.3V regulator simultaneously, to avoid unbalanced loading. The stepper and servo connectors utilized USBC connectors as well but did not use the USB protocol. USBC connectors were chosen over other USB connectors because of the higher power delivery capabilities of the connector. This enabled the utilization of cheap commercially available connectors without the overhead of components required for the USB protocol. The servo controller on the servo board was instead communicated to using I^2C, and delivered 5V, through a power switch IC enabled with a GPIO. The utilization of power switch ICs allowed the the peripheral boards to be de-powered, reducing the power draw from those components when not needed. Likewise, the stepper controller board was intended to be connected via USBC, sending the direction and clock data directly to the stepper controller over the USB connector. However, due to issues with the board discussed in the testing section, this was not utilized. The sensor board was connected with USBA as the power draw from the sensors was minimal and USBA connectors were far cheaper than USBC. The sensor board would be communicated with utilizing I^2C. Also included on the MCU board were 2 TPS54JA20 buck regulators, that would step the 12V line from the charge controller down to a usable 3.3V and 5V respectively. A comparator, A PTC fuse was utilized to ensure safe operation of the board and to reduce the likelihood of damage in the case of a short to ground. A comparator, Zener diodes, and LEDs were included as voltage indicators to simplify troubleshooting and to indicate whether the 3.3V and 5V lines were powered. A PTC fuse was utilized to ensure safe operation of the board and to reduce the likelihood of damage in the case of a short to ground. Throughout the board were jumper headers for various GPIOs, power lines and data lines, enabling easy troubleshooting. This proved invaluable during the testing process, as discussed in the testing section. Another revision of the MCU board was manufactured, to resolve some minor issues that occurred.

2) Servo Controller Board: The servo controller board was rather simple. A 5V LDO regulator would step down the 5V received from the USBC connector to the servo controller itself. The I^2C data and clock lines were connected to the controller and pullup resistors. The 5V, GND, and the PWM line from the servo controller were connected to jumper headers for the servos to connect to.

3) Sensor Board: The sensor board was another rather simple board. This board featured five VEML7700 sensors, an 8-channel MUX and a USB connector. The 8-channel MUX was necessary because the VEML sensors come with the same I^2C address by default, and this cannot be altered. To circumvent this, a TCA9548A 8-channel I^2C MUX was used. This enabled us to address each sensor individually, by changing which line was open on the MUX before addressing the sensor. The USB-A connector delivered 3.3V, I^2C data, clock and GND. The 5 sensors were placed on the board in a manner such that the sensor partition shown in Fig. 1 would be placed evenly between them. A switch was included on the sensor board to enable resetting the MUX during testing.

4) Stepper Controller Board: A stepper controller board was initially designed, however it proved faulty later. The first stepper controller board featured a controller that did not deliver enough current to drive the stepper, however functioned fine otherwise. The second revision of the board proved faulty, as discussed in the testing section. The second revision featured a USBC connector to connect to the MCU board and terminal connectors for testing. It was designed to operate on 12V from the charge controller and

utilized a TB6560 as the controller. Optocouplers were utilized to isolate signals in conjunction with sensitive ICs, such as a CD74HC123 CMOS Multivibrators to ensure the stepper held its position when not actively stepping. The design was based on the devkit utilized but again, proved faulty.

V. Software

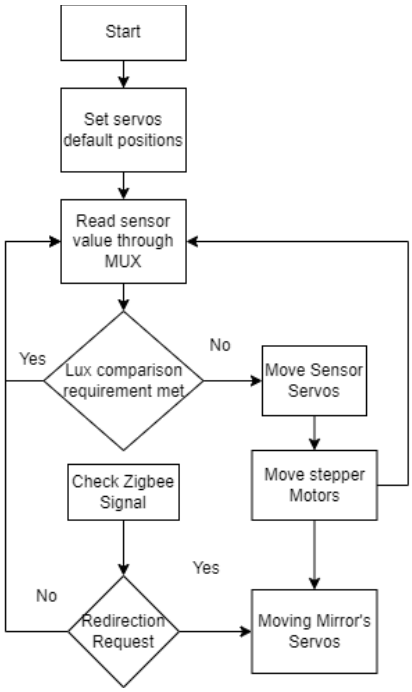

Fig. 5. Overall software logic diagram.

A. Ray Tracing Algorithm

The implementation of a solar tracking system involves precise adjustments of both horizontal and vertical components to effectively track the sun's position. The algorithm devised for horizontal tracking utilizes sensor data to dynamically adjust the stepper motor controlling the base of the tower. By analyzing sensor inputs and applying mathematical transformations, the algorithm ensures continuous and accurate movement of the base to maintain alignment with the sun's position. Similarly, the vertical adjustment of the mirror is achieved by correlating sensor servo movements and horizontal adjustments from stepper movements with the positioning of the mirror, adhering to Snell's law of reflection. Scaling operations are employed to translate sensor data using step sizes into precise vertical scaling in (3) and horizontal scaling in (4) for movements of the mirror, ensuring optimal reflection of sunlight towards the target:

$$v_m = \frac{(v_s - 495)(400-600)}{765-495} + 600, \quad (3)$$

$$h_m = \frac{h_t(300-510)}{1440} + 510. \quad (4)$$

B. Mesh Network Control

Incorporating the mesh network functionality through Zigbee communication protocols enhances the versatility of the solar tracking system. Leveraging the tower as a receiver allows real-time adjustment of the mirror's target position via signals transmitted through the mesh network. By storing target values in an array and toggling between them based on received signals, the system demonstrates seamless integration of multiple towers within the network. This integration facilitates efficient coordination and synchronization among different components, showcasing the system's adaptability and responsiveness to changing environmental conditions.

VI. Testing

A. Ray Tracing Algorithm

The functionality of various components for the project was tested to ensure proper operation. Firstly, the ESP32-C6 development boards were tested by powering them through USB-C ports and verifying GPIO pin voltages with a digital multimeter, as well as confirming reset button functionality. Similarly, the AdaFruit MicroSD card breakout board was tested by connecting it to the ESP32-C6 and inserting a microSD card, followed by readiness testing of the file system software. The hardware functionality of the VEML7700 light sensor was tested by wiring it to the ESP32-C6 and confirming proper connections, both physically and through software testing to ensure data transfer. The TCA9548A I2C Multiplexer underwent similar hardware testing, with connections to the microcontroller and sensors, ensuring proper data transfer through GPIO pins.

Additionally, the mechanical components were tested, including two servo motors attached for precise rotation of the reflector on the x and y axes, and another servo motor for vertical rotation based on sensor input. A stepper motor was used for the w axis, enabling rotation of the entire structure. Modifications to the ESP32-C6 development boards for antenna connections were noted, with possibilities for external antenna soldering. Simulations were conducted on the PCB designs, refining LED indicator circuits and voltage regulators through theoretical testing using tools like Fadstad circuits and TI Webench.

Furthermore, the charge controller underwent testing powered by a DC power supply, addressing initial issues with over-voltage protection by configuring it specifically for LiFePo batteries. Real-world testing under load conditions is required to further validate its operation.

Similarly, the solar panel was tested outdoors, yielding the expected voltage output, but further testing under load conditions is necessary to ensure functionality in real-world scenarios.

During testing of the integration, there were multiple issues and errors encountered that were solved to effectively complete the project in a timely manner. Some of these issues were, but were not limited to, Inter-Integrated Circuit (I^2C) rise times issues, faulty Zigbee coordinator equipment, issues pairing the ESP32-C6 to the Zigbee coordinator frontend, problems interfacing the multiplexer using software to control the sensors, and revisions to PCB design.

B. I^2C Issues

Some of the issues with I^2C were due to higher than anticipated capacitance on the channel, resulting in slow rise time of signal pulses. These issues were resolved by reducing the clock rate of the I^2C signal where possible, and where not possible, by reducing the resistance of pull-up resistors, whilst still considering the maximum current draw tolerable from the ESP32-C's GPIO pins.

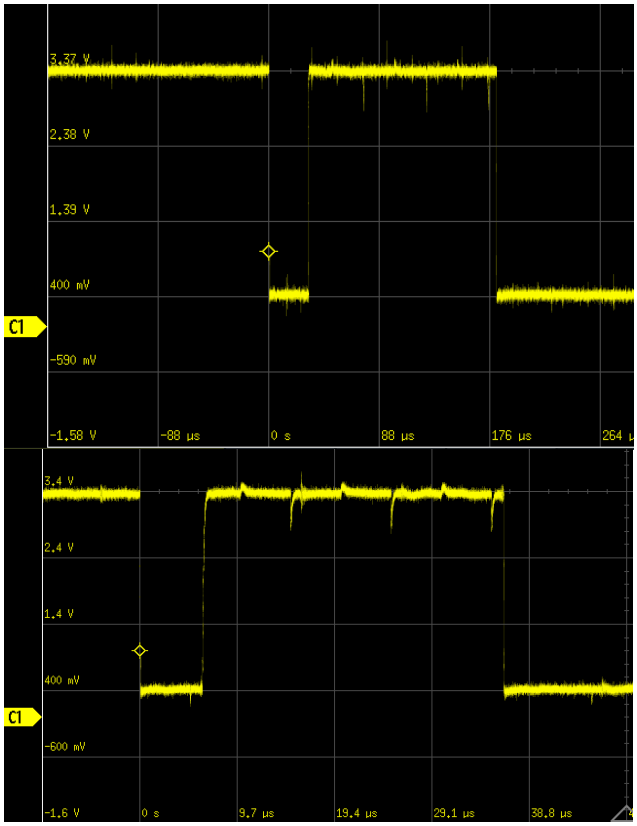

Fig. 6. The I2C issue shown from an oscilloscope. The low frequency signal (shown above) shows the improvement in relative rise time over the high frequency signal (shown bottom).

C. Mesh Networking Issues

The development of the mesh network faced a few major hurdles that had to be overcome. The first problem was a very rare issue with the first Zigbee coordinator dongle in which the UART bridge did not work, making it impossible to communicate with. This was understood by careful testing with an oscilloscope and a terminal attempting to send to the IC through the UART bridge. This was resolved by purchasing a new dongle.

The subsequent hurdles involved getting the hardware to work together. Using Zigbee2MQTT was a great help but also added challenges into the project. Getting the ESP32-C6 to pair with the coordinator hosted by Zigbee2MQTT was not a straightforward process but was eventually resolved by clearing cache on the microcontroller and working with the Zigbee2MQTT front end.

The other major issue was getting Zigbee2MQTT to see the microcontroller as a supported device. It is not an officially supported device since it can theoretically be coded to do anything. Due to this, it was required to check how the configuration files were set up for other similar devices so that it could be configured and interacted with properly.

D. FreeRTOS Issues

Another issue faced was trying to read from multiple light sensors in a row using the I^2C multiplexer using C code. Some of the issues faced while trying to create this using the ESP-IDF framework was that it was constantly going through software resets when reading from each sensor, due to issues from the FreeRTOS implementation that was used in previous example codes for similar products. It was ultimately decided to completely remove these libraries and code using them to create a custom channel select for the multiplexer to simplify the code.

E. Voltage Sag Issues

Another challenge faced was the current draw from the servos causing a large drop in voltage on the servo boards 5V line. This would propagate down to the 3.3V line as the LDO regulator would not be able to operate below its dropout voltage. This would drop the enable pin on the servo controller below a logic 1, result in a brief inability to communicate to the servo controller, and a need to initialize the servo controller. In Fig.6 the issue can be seen visually. After some troubleshooting, the issue was determined to be cause by I^2R losses across a rather narrow trace, in addition to utilizing a lab power supply rather than the intended regulator. This resulted in the voltage sensing of the regulator being unable to maintain 5V at the distant servo controller board. This was resolved by using a conjunction

of methods. The required current draw was reduced from the servo motors by reducing the instantaneous change in angle using software. The intended regulator was also installed, reducing the I^2R losses and moving the voltage sense closer to the servo controller board. The combination of these changes resulted in this issue being resolved.

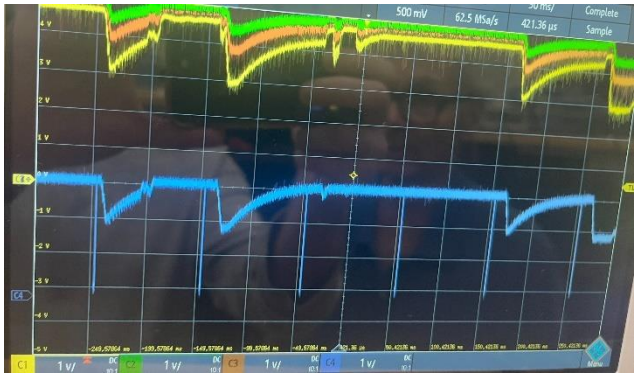

Fig. 7. The I^2R losses visualized. In green is a measurement of voltage nearest the 5V regulator while the servos are running, and increasing in distance from the regulator are the orange and yellow respectively. The blue plot is the 3.3V I^2C line. As can be seen the 3.3V line is impacted by the I^2R losses on the 5V line due to the servos moving. The vertical discontinuities in the blue plot are the I^2C signals being sent.

F. PCB Revision Issues

Some other design errors resulted in a desire to revise the initial MCU board. A mix-up between the TX and RX pins on the output of the USB/UART converter caused the device to detect the UART converter but not able to communicate to the ESP. In our first design the MCU board had the TX pin from the MCU connected to the TX pin of the UART converter and likewise for the RX pins. We were able to resolve this due to the prudent inclusion of jumper headers for the TX and RX pins, allowing us to use jumpers to bridge the pins. Another issue was a mix-up in the strapping pins. The GPIO pins that the ESP32-C6 uses for strapping pins differs between the Dev-kit and the standalone MCU. These differences resulted in the need to utilize jumpers to the strapping GPIO pins of the ESP, which was inelegant. This resulted in being unable to boot into the MCU. Again, the prudent inclusion of jumper headers for the GPIOs, enabled jumpers to be used to manually raise and lower the strapping pins, putting the ESP into and out of boot mode. The combination of these issues proved tedious and resulted in the desire to revise the board to solve these issues. The revision included a switch for to raise and lower the strapping pins to reduce time spent flashing code, enabling faster iterations of software, as well as fixing some other minor issues, such as the TX/RX mix-up and refining some footprints, silkscreen, and component placement.

G. Stepper Issues

The initial stepper board worked, however only unloaded. Once the stepper had a load applied to it, the stepper would stall. This was due to the stepper controller being too small for the application. The second revision of the board featured a TB6560 controller. A development kit was tested under load and functioned fine, however after implementing a similar design on a PCB, the stepper mototr had insufficient drawn in current when utilizing fabricated board. Only a tenth of the needed current was able to be drawn compared to development board. The issue is believed to be due to the current limiting resistors being of the wrong value, however this is untested. The group opted to utilize the development kit instead of troubleshooting the second iteration of the stepper controller board, to reduce costs of manufacturing another revision and reduce design time.

VII. Conclusion

In conclusion, ASTROCOM project demonstrated the solar reflector system and mesh network functions as expected and meets specified requirements. The power output of the system is sustainable for an extensive period of use. The reflection angles ranges are wide enough to have a large area of coverage. However, there exist many opportunities for improvement through the integration of photonics' and mechanicals' expertise. Enhancements such as improved rotation mechanisms, advanced materials for reflecting sunlight, and optimized solar reflector algorithms can significantly enhance the system's performance.

Furthermore, by scaling up in term of funding and placing the materials to meet constrained environments, notable improvements can be achieved. For instance, utilizing gold alloy for mirror construction, or employing aluminum and mylar coatings instead of plastic and adhesive for mirror manufacturing. Parts' housing can incorporate carbon fiber to enhance both efficiency, weight, and durability. Additionally, protective measure can implement by insulation to the computer board. Transitioning to industrial servos capable of withstanding high heat fluctuations is essential for ensuring reliable operation in challenging conditions.

Mesh network can be expanded be integrating router nodes throughout the network architecture. Additional Zigbee commands can be implemented to increase the network's functionality. Image's packages can be move

through the network and temporary stored in the implemented storage of the designed board.

In summary, while the current solar reflector system meets basic requirements, ongoing research and development efforts focused on integrating advanced technologies and materials will be instrumental in optimizing its performance and expanding its potential applications.

ACKNOWLEDGEMENT

The authors would like to acknowledge the support of Chan Chung Yong, PhD and Arthur Weeks, PhD first and foremost for their unrelenting support and mentoring throughout the project's planning and implementation.

Also deserving of recognition is the Florida Space Institute as the project's sponsor with Mr. Mike Conroy as the main agent providing funding and support for the project as well as keeping track of the project's progress, objectives and goals.

The University of Central Florida has graciously provided the excellent facilities that allowed for efficient work on the project such as the Senior Design Lab, Junior Design Lab and the Texas Instruments Innovation Lab.

Last but not least, a thanks to the reviewers that agreed to be on our project's committee: Mike Borowczak, PhD, Mingjie Lin, PhD, and Saleem Sahawneh, PhD.

BIOGRAPHY

Alexandre Fiset is a senior in Electrical Engineering at UCF set to graduate in May 2024. He has previous experience working as a student intern at the Orlando Utilities Commission and is currently engaging in undergraduate research in DER Cybersecurity with the RISES Center at UCF. He plans to continue his education, seeking a master's degree in electrical engineering from UCF.

Pedro Kasprzykowski is a senior in Computer Engineering, Comprehensive Track at the University of Central Florida set to graduate in May 2024. He will be starting a PhD in Computer Science at the University of Colorado Boulder in August 2024. His long-term goal is a career in teaching as a university faculty member.

Stephen Martin is a current senior set to graduate in May 2024 with a degree in Computer Engineering, Comprehensive Track from the University of Central Florida (UCF). He plans to pursue graduate school at UCF studying Engineering Management while remaining a member of the UCF football team.

Binh Pham is a senior Computer Engineer student in VLSI track at the University of Central Florida. He will finish his undergraduate studies in May 2025 and continue to pursue a master's degree in the same field and graduate in May 2024. His career goal is to incorporate Engineer and Chemistry in biomedical industry.

REFERENCES

[1] A. Sánchez-González and J. Yellowhair, "Reflections between heliostats: Model to detect alignment errors," Solar Energy, vol. 201, pp. 373–386, May 2020, doi: https://doi.org/10.1016/j.solener.2020.03.005.

[2] "ESP32-Devkitc." *ESP32-DevKitC Board I Espressif*, www.espressif.com/en/products/devkits/esp32-devkitc. Accessed 24 Nov. 2023. "ESP32-Devkitc." ESP32-DevKitC Board I Espressif, www.espressif.com/en/products/devkits/esp32-devkitc. Accessed 24 Nov. 2023.

[3] VEML7700, Vishay Semiconductors, 28 Apr. 2022, www.vishay.com/docs/84286/veml7700.pdf.

[4]